^{19}F NMR Spectra and Structures of Halogenated Porphyrins

Eva R. Birnbaum, Julia A. Hodge, Mark W. Grinstaff, William P. Schaefer, Lawrence Henling, Jay A. Labinger,* John E. Bercaw,* and Harry B. Gray*

Arthur Amos Noyes Laboratory,† California Institute of Technology, Pasadena, California 91125

Received November 4, 1994⊗

Fluorine-19 NMR spectra of a series of halogenated porphyrins have been used to create a spectral library of different types of fluorine splitting patterns for tetrakis(pentafluorophenyl) porphyrins (TFPP) complexed with diamagnetic and paramagnetic metal ions. The paramagnetic shift, line broadening, and fine structure of the resonances from the peripheral pentafluorophenyl rings are dependent on the symmetry and core environment of the porphyrin macrocycles. In combination with crystal structure data, ^{19}F NMR helps define the behavior of halogenated porphyrins in solution. Six new crystal structures for TFPP and octahalo-TFPP derivatives are reported: H_2TFPP in rhombohedral space group $R\bar{3}$, a = 20.327(4) Å, c = 24.368(5) Å, V = 8720(3) Å^3, Z = 9; ZnTFPP in monoclinic space group $P2_1/c$, a =12.653(4) Å, b = 11.883(5) Å, c = 15.261(2) Å, β = 103.87(2)°, V = 2227.6(13) Å^3, Z = 2; CuTFPP in rhombohedral space group $R\bar{3}$, a = 20.358(5), c = 24.347(6) Å, V = 8739(4) Å^3, Z = 9; H_2TFPPCl$_8$ in triclinic space group $P\bar{1}$, a = 11.066(1) Å, b = 14.641(3) Å, c = 14.678(2) Å, α = 88.97(1), β = 76.05(1)°, γ = 71.29(1)°, V = 2181.4(6) Å^3, Z = 2; ZnTFPPCl$_8$ in tetragonal space group $P\bar{4}2_1c$, a = 19.502(20), c = 10.916(8) Å, V = 4152(6) Å^3, Z = 2; H_2TFPPBr$_8$ in monoclinic space group $C2$, a = 27.634(6) Å, b = 6.926(2) Å, c = 14.844(3) Å, β = 109.64(2)°, V = 2675.8(11) Å^3, Z = 2.

Extensive investigations have established that halogenated metalloporphyrins are robust catalysts for hydrocarbon oxygenations.[1-16] β-Haloporphyrins with mesityl, 2,6-dihalophenyl, or pentafluorophenyl groups at the *meso* positions are among the most active complexes. These porphyrins share several of the unusual properties related to catalytic activity: the resistance to oxidative degradation,[5,17,18] positively shifted electrochemical potentials,[19-22] and remarkably distorted structures.[23-26] Although the tetramesityl and 2,6-dihalo derivatives are generally well characterized by ^1H NMR, identification of the perhalogenated pentafluorophenyl derived porphyrins is hampered by the lack of protons on the molecule. We have found that ^{19}F NMR spectroscopy is a useful adjunct to crystal structure analysis for characterization purposes. Here we report the NMR spectra and molecular structures of six halogenated derivatives of tetraphenylporphyrin: 5,10,15,20-tetrakis(pentafluorophenyl)-porphyrin (H_2TFPP) and its zinc and copper complexes (5,10,15,20-tetrakis(pentafluorophenyl)porphyrinato)-zinc(II) (ZnTFPP) and (5,10,15,20-tetrakis(pentafluorophenyl)-porphyrinato)copper(II) (CuTFPP); the completely halogenated 2,3,7,8,12,13,17,18-octa-β-chloro-5,10,15,20-tetrakis(pentafluorophenyl)porphyrin (H_2TFPPCl$_8$) and its zinc complex (2,3,7,8,12,13,17,18-octa-β-chloro-5,10,15,20-tetrakis-(pentafluorophenyl)porphyrinato)zinc(II) (ZnTFPPCl$_8$); and 2,3,7,8,12,13,17,18-octa-β-bromo-5,10,15,20-tetrakis(pentafluorophenyl)porphyrin (H_2TFPPBr$_8$). These compounds are precursors to the catalytically active iron porphyrins.[1,13] Comparisons with NMR spectra of other structurally characterized[27-29] (tetrakis(pentafluorophenyl)porphyrinato)iron(III) complexes are extended to facilitate characterization of other metalated derivatives.

†Contribution No. 9005.

⊗ Abstract published in *Advance ACS Abstracts,* June 1, 1995.

(1) Ellis, P. E., Jr.; Lyons, J. E. *Catal. Lett.* **1989**, *3*, 389–398.
(2) Ellis, P. E., Jr.; Lyons, J. E. *Coord. Chem. Rev.* **1990**, *105*, 181–193.
(3) Lyons, J. E.; Ellis, P. E., Jr.; Durante, V. A. In *Structure-Activity and Selectivity Relationships in Heterogeneous Catalysis*; Grasselli, R. K., Sleight, A. W., Eds.; Elsevier Science Publishers BV: Amsterdam, 1991; pp 99–116.
(4) Lyons, J. E.; Ellis, P. E., Jr.; Myers, H. K., Jr.; Wagner, R. W. *J. Catal.* **1993**, *141*, 311–315.
(5) Traylor, P. S.; Dolphin, D.; Traylor, T. G. *J. Chem. Soc., Chem. Commun.* **1984**, 279–280.
(6) Traylor, T. G.; Tsuchiya, S. *Inorg. Chem.* **1987**, *26*, 1338–1339.
(7) Traylor, T. G.; Hill, K. W.; Fann, W.; Tsuchiya, S.; Dunlap, B. E. *J. Am. Chem. Soc.* **1992**, *114*, 1308–1312.
(8) Hoffmann, P.; Meunier, B. *New J. Chem.* **1992**, *16*, 559–561.
(9) Bartoli, J. F.; Brigaud, O.; Battioni, P.; Mansuy, D. *J. Chem. Soc., Chem. Commun.* **1991**, 440–442.
(10) Banfi, S.; Mandelli, R.; Montanari, F.; Quici, S. *Gazz. Chim. Ital.* **1993**, *123*, 409–415.
(11) d'A. Rocha Gonsalves, A. M.; Johnstone, R. A. W.; Pereira, M. M.; Shaw, J.; Sobral, D. N.; Abilio, J. F. *Tetrahedron Lett.* **1991**, *32*, 1355–1358.
(12) Nappa, M. J.; Tolman, C. A. *Inorg. Chem.* **1985**, *24*, 4711–4719.
(13) Grinstaff, M. W.; Hill, M. G.; Labinger, J. A.; Gray, H. B. *Science* **1994**, *264*, 1311–1313.
(14) Labinger, J. A. *Catal. Lett.* **1994**, *26*, 95–99.
(15) Maldotti, A.; Bartocci, C.; Amadelli, R.; Polo, E.; Battioni, P.; Mansuy, D. *J. Chem. Soc., Chem. Commun.* **1991**, 1487–1489.
(16) Shelnutt, J. A.; Trudell, D. E. *Tetrahedron Lett.* **1989**, *30*, 5231–5234.
(17) Ellis, P. E., Jr.; Lyons, J. E. *J. Chem. Soc., Chem. Commun.* **1989**, 1315–1316.
(18) Chang, C. K.; Ebina, F. *J. Chem. Soc., Chem. Commun.* **1981**, 778–779.
(19) Birnbaum, E. R.; Schaefer, W. P.; Labinger, J. A.; Bercaw, J. E.; Gray, H. B. *Inorg. Chem.* **1995**, *34*, 1751–1755.
(20) Ochsenbein, P.; Ayougou, K.; Mondon, D.; Fischer, J.; Weiss, R.; Austin, R. N.; Jayaraj, K.; Gold, A.; Terner, J.; Fajer, J. *Angew. Chem.* **1994**, *33*, 348–350.
(21) Takeuchi, T.; Gray, H. B.; Goddard, W. A., III. *J. Am. Chem. Soc.* **1994**, *116*, 9730–9732.
(22) Hodge, J. A.; Hill, M. G.; Gray, H. B. *Inorg. Chem.* **1995**, *34*, 802–812.
(23) Henling, L. M.; Schaefer, W. P.; Hodge, J. A.; Hughes, M. E.; Gray, H. B.; Lyons, J. E.; Ellis, P. E., Jr. *Acta Crystallogr.* **1993**, *C49*, 1745–1747.
(24) Schaefer, W. P.; Hodge, J. A.; Hughes, M. E.; Gray, H. B.; Lyons, J. E.; Ellis, P. E., Jr.; Wagner, R. W. *Acta Crystallogr.* **1993**, *C49*, 1342–1345.
(25) Marsh, R. E.; Schaefer, W. P.; Hodge, J. A.; Hughes, M. E.; Gray, H. B.; Lyons, J. E.; Ellis, P. E., Jr. *Acta Crystallogr.* **1993**, *C49*, 1339–1342.
(26) Mandon, D.; Ochsenbein, P.; Fischer, J.; Weiss, R.; Jayaraj, K.; Austin, R. N.; Gold, A.; White, P. S.; Brigaud, O.; Battioni, P.; Mansuy, D. *Inorg. Chem.* **1992**, *31*, 2044–2049.
(27) Longo, F. R.; Finarelli, M. G.; Kim, J. B. *J. Heterocycl. Chem.* **1969**, *6*, 927–931.

0020-1669/95/1334-3625$09.00/0 © 1995 American Chemical Society

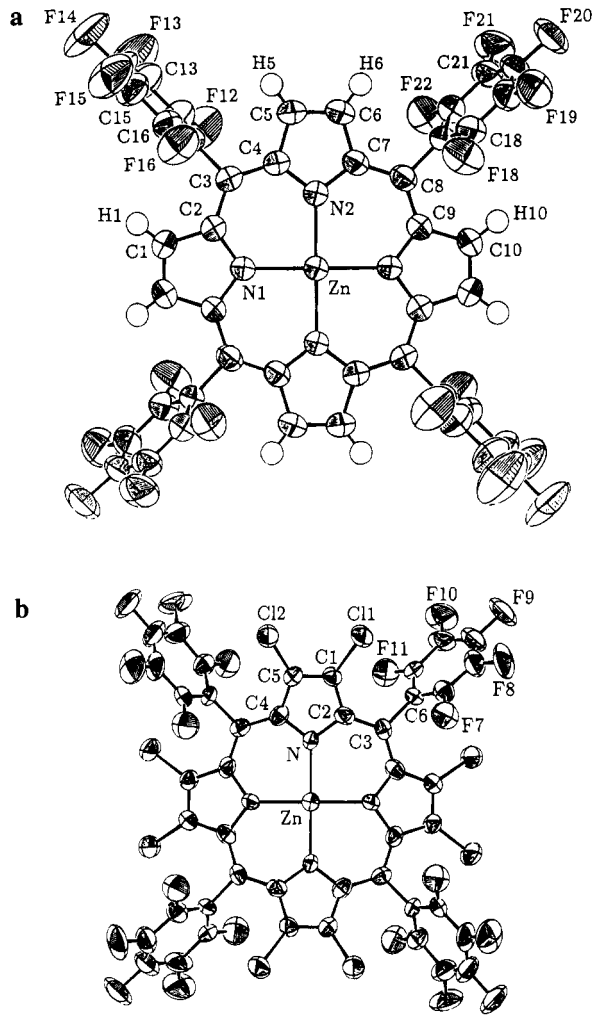

Figure 1. ORTEP drawings of (a) ZnTFPP and (b) $ZnTFPPCl_8$ with 50% probability ellipsoids. Other ORTEPs are included in the supporting information.

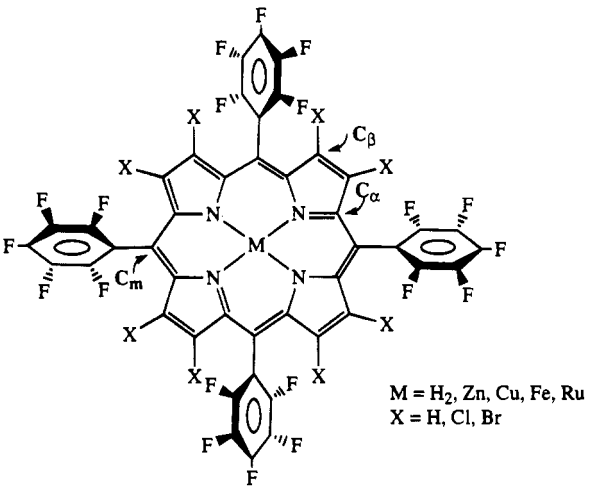

Figure 2. A diagram of the porphyrins described in the paper, with the α-, β-, and *meso*-carbons indicated. For the crystallized porphyrins, M = H_2, Zn, Cu and X = H, Cl, Br.

Results and Discussion

Molecular Structures. Representative ORTEP diagrams for the TFPP and $TFPPX_8$ (X = Cl, Br) complexes are shown in Figure 1, with the atom-labeling system defined in Figure 2. ORTEPs for the remaining four complexes are included in the supporting information (formerly known as supplementary material). The three essentially planar TFPP complexes crystallized in space groups $R\bar{3}$ (H_2 and Cu) and $P2_1/c$ (Zn) (Table 1). ZnTFPP crystallized with a hexane molecule in the unit cell. The isostructural H_2 and Cu complexes crystallized without solvent molecules in the lattice.

$H_2TFPPCl_8$ crystallized in space group $P\bar{1}$, with two porphyrins in the unit cell. The two parallel porphyrin molecules are 4.74 Å apart, with the porphyrin centers slightly offset (center to center distance 6.1 Å). The zinc derivative, $ZnTFPPCl_8$, crystallized with *o*-dichlorobenzene molecules in roughly parallel planes on either side of the porphyrin molecule. The solvent molecules are located 3.4 Å from the mean plane of the porphyrin, a distance suggestive of a π-stacking interaction between the π systems of the porphyrin and the *o*-dichlorobenzene molecules. Aromatic solvent molecules were found to stack in a similar fashion in the crystal structure of (tetraphenylporphyrinato)zinc(II) bis(toluene), $ZnTPP(C_6H_5CH_3)_2$, where two toluene molecules occupy these positions.[30] The π donor ability of the aromatic solvent may help stabilize the zinc ion in the electron deficient macrocycle. Similarly, $H_2TFPPBr_8$ was found to crystallize with an *o*-dichlorobenzene molecule stacked above each porphyrin molecule.

Remarkably, bond lengths (Table 2) in the porphyrin skeleton are essentially preserved throughout the series of metallo derivatives of TPP,[30-32] TFPP, and $TFPPX_8$ (X= Cl, Br). A notable trend in the structures is the decrease in the $C_\alpha-N-C_\alpha$ and $C_\alpha-C_m-C_\alpha$ angles in the series H_2TFPP, ZnTFPP, CuTFPP (Table 3). This is likely due to an increasing contraction of the porphyrin macrocycle as the metal−nitrogen bond length decreases. Average M−N bond lengths in Zn and Cu pyrrole complexes decrease from 2.068 to 1.991 Å,[33] comparable to the metal to nitrogen distance decrease from 2.036 to 1.996 Å, respectively, from ZnTFPP to CuTFPP. The distorted $TFPPX_8$ complexes share both of these trends, demonstrating that, in many respects, the planar and distorted structures are surprisingly similar.

Addition of chlorine or bromine to the pyrrole β-carbons induces severe tetrahedral distortions (Figures 3 and 4), reducing the molecular symmetry from D_{4h} to D_2. The pairs of β-halogen atoms are located alternately above and below the average plane determined by the four central nitrogen atoms, and the phenyl rings are rotated slightly toward the mean porphyrin plane to minimize steric contact between the halogen atoms at the pyrrole positions and the *o*-carbons of the pentafluorophenyl rings. The distortion of the macrocycle is specifically quantified in Table 4 as the distances of the *meso*- and β-carbons from the mean plane of the porphyrin (defined as the average plane of the four core nitrogen atoms). A view of the free ligand porphyrins H_2TFPP, $H_2TFPPCl_8$, and $H_2TFPPBr_8$ (Figure 3), generated from crystal structure coordinates, shows the increasing distortion along the series.

Two types of distortion are observed, analogous to those

(28) Jayaraj, K.; Gold, A.; Toney, G. E.; Helms, J. H.; Hatfield, W. E. *Inorg. Chem.* **1986**, *25*, 3516−3518.
(29) Gold, A.; Jayaraj, K.; Doppelt, P.; Fischer, J.; Weiss, R. *Inorg. Chim. Acta* **1988**, *150*, 177−181.
(30) Scheidt, W. R.; Kastner, M. E.; Hatano, K. *Inorg. Chem.* **1978**, *17*, 706−710.
(31) Hoard, J. L. *Ann. N.Y. Acad. Sci.* **1973**, *206*, 18−31.
(32) Fleischer, E. B.; Miller, C. K.; Webb, L. E. *J. Am. Chem. Soc.* **1964**, *86*, 2342−2347.
(33) Orpen, A. G.; Brammer, L.; Allen, F. H.; Kennard, O.; Watson, D. G.; Taylor, R. *J. Chem. Soc., Dalton Trans.* **1989**, S1-S83.

Table 1. X-ray Experimental Parameters[a]

	$H_2TFPPCl_8$	$ZnTFPPCl_8$	$H_2TFPPBr_8$	H_2TFPP	ZnTFPP	CuTFPP
formula	$C_{44}H_2Cl_8F_{20}N_4$	$C_{44}Cl_8F_{20}N_4Zn \cdot 6C_6H_4Cl_2$	$C_{44}H_2Br_8F_{20}N_4 \cdot C_6H_4Cl_2$	$C_{44}H_{10}F_{20}N_4$	$C_{44}H_8F_{20}N_4Zn \cdot C_6H_{14}$	$C_{44}H_8F_{20}N_4Cu$
mol wt	1250.12	2139.48	1752.73	982.57	1124.10	1044.10
color	brown	dull red	dark brown	red brown	pink	ruby red
shape	plate	thick needles	thin plate	plate	thick needles	plate
crystal system	triclinic	tetragonal	monoclinic	rhombohedral	monoclinic	rhombohedral
space group	$P\bar{1}$	$P\bar{4}2_1c$	$C2$	$R\bar{3}$	$P2_1/c$	$R\bar{3}$
a, Å	11.066(1)	19.502(20)	27.634(6)	20.327(4)	12.653(4)	20.358(5)
b, Å	14.641(3)		6.926(2)		11.883(5)	
c, Å	14.678(2)	10.916(8)	14.844(3)	24.368(5)	15.261(2)	24.347(6)
α, deg	88.97(1)					
β, deg	76.05(1)		109.64(2)		103.87(2)	
γ, deg	71.29(1)					
V, Å^3	2181.4(6)	4152(6)	2675.8(11)	8720(3)	2227.6(13)	8739(4)
Z	2	2	2	9	2	9
Dx, g cm^{-3}	1.90	1.71	2.18	1.67	1.68	1.77
μ, cm^{-1}	6.4	10.41	61.52	1.60	4.91	6.96
temp, K	293	229	225	298	296	295
crystal size, mm	0.11 × 0.35 × 0.42	0.19 × 0.19 × 0.59	0.07 × 0.23 × 0.50	0.19 × 0.35 × 0.36	0.18 × 0.27 × 0.56	0.28 × 0.52 × 0.54
$h_{min/max}$	±12	0/23	0/32	±24	±15	±28
$k_{min/max}$	±16	0/23	±8	±24	±14	±28
$l_{min/max}$	±16	±13	±17	±28	0/18	±34
no. of reflns measd	12455	8027	4881	7209	8421	12512
no. of indep. reflns	6054	2050	4710	3403	3902	5651
no. of reflns used	6054	2050	4710	3403	3902	5651
$R_{int}(F)$	0.019	0.033	0.041	0.043	0.028	0.038
$R(F)$	0.034	0.078	0.043	0.047	0.038	0.049
$R_w(F_2)$	0.0061	0.0286	0.006	0.011	0.007	0.009
$(\Delta/\sigma)_{max}$	0.01	0.07	0.10	0.01	0.10	0.01
goodness of fit	2.05	3.29	1.41	1.78	1.95	1.99

[a] Mo Ka radiation, 0.7107 Å; Enraf-Nonius CAD-4 diffractometer.

Table 2. Selected Average Bond Lengths (Å)

	$H_2TFPPCl_8$	$ZnTFPPCl_8$	$H_2TFPPBr_8$	H_2TFPP	ZnTFPP	CuTFPP
N−C_α	1.372	1.380	1.368	1.369	1.371	1.376
C_α−C_β	1.448	1.427	1.456	1.438	1.438	1.437
C_β−C_β	1.347	1.337	1.348	1.329	1.339	1.334
C_α−C_m	1.402	1.403	1.411	1.393	1.398	1.387
H−N	0.94			0.91		
M−N		2.032			2.036	1.996
Ct−N[a]	2.075	2.029	2.0252, 2.0602	2.0166, 2.0882	2.036	1.996

[a] Core size (defined as the distance between the center of the molecule and a projection of the nitrogen atoms onto the porphyrin plane).

Table 3. Selected Average Bond Angles (deg)

	$H_2TFPPCl_8$	$ZnTFPPCl_8$	$H_2TFPPBr_8$	H_2TFPP	ZnTFPP	CuTFPP
C_α−N−C_α	109.5	106.9	108.8	107.4	106.2	105.2
N−C_α−C_m	125.4	124.2	124.0	125.4	125.1	125.2
N−C_α−C_β	107.2	107.4	108.1	108.5	109.6	110.2
C_α−C_β−C_β	107.9	108.8	107.4	107.2	107.3	107.2
C_α−C_m−C_α	125.8	126.5	124.6	127.2	126.1	124.81
C_m−C_α−C_β	127.2	128.4	127.6	126.4	125.4	124.6
dihedral (C_6F_5 groups)	72.6	59.1	54.3	79	72.6	78
N1−M−N2		90.2			89.8	90.4
N1−M−N3		174.1			179.6	180

reported by Scheidt and Lee:[34] "ruffling" or twist (distortion manifested at the *meso*-carbons) and "saddling" (distortion manifested at the β-carbons). Relative to the planar H_2TFPP, $H_2TFPPCl_8$ has a substantial saddle distortion. Substitution with larger bromine atoms enhances this effect; the average C_β displacement from the plane increases from 0.051 to 0.62 to 0.90 Å in this series. The free ligand, $H_2TFPPCl_8$, is the least distorted of the structurally characterized chlorinated porphyrins [$ZnTFPPCl_8$, $CuTFPPCl_8$,[24] $RuTFPPCl_8(CO)H_2O$[19]], as reflected by the smaller perpendicular displacements of atoms from the mean porphyrin plane and a lack of the twisting or ruffling observed in the metalated derivatives. The saddle distortion is smaller in the free ligand (average C_β displacement = 0.62 Å) than in the metalated derivatives $ZnTFPPCl_8$ (0.75 Å) and $CuTFPPCl_8$ (0.70 Å)[24] but greater than in the octahedrally coordinated $RuTFPPCl_8(CO)H_2O$ (0.48 Å).[19] The saddle distortion of the brominated porphyrins, again assessed by C_β displacement, consistently increases as the core size decreases: $H_2TFPPBr_8$ (0.90), $ZnTFPPBr_8$ (0.97),[25] $CuTFPPBr_8$ (1.12),[23] and $NiTFPPBr_8$ (1.17 Å).[26]

Though saddled, the unmetalated $H_2TFPPCl_8$ has essentially no twist distortion (average C_m displacement = 0.023 Å). The increase in the van der Waals radius by 0.15 Å from chlorine to bromine, however, generates enough steric bulk on the pyrrole rings to induce a slight twist in $H_2TFPPBr_8$ (0.091 Å). When

(34) Scheidt, W. R.; Lee, Y. J. In *Metal Complexes with Tetrapyrrole Ligands I*; Buchler, J. W., Ed.; Springer-Verlag: New York, 1987; Vol. 64; pp 2−70.

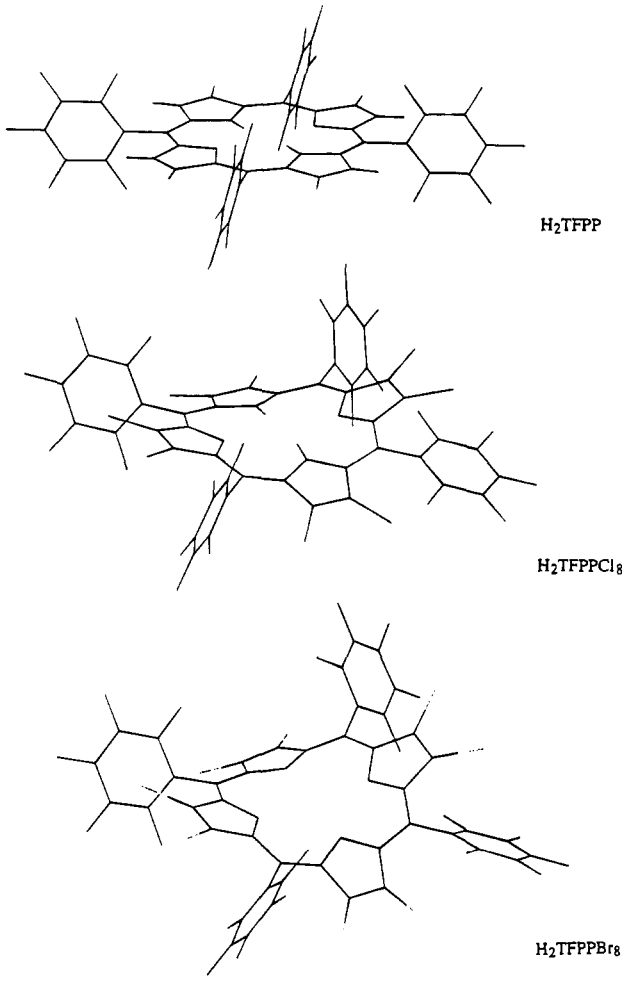

Figure 3. Molecular representations of the series H_2TFPP, $H_2TFPPCl_8$, and $H_2TFPPBr_8$ using the crystal structure coordinates. From the planar H_2TFPP, the saddle distortion clearly increases upon further halogenation.

the metal atom sits inside the core, a large twist distortion is observed: $ZnTFPPCl_8$ (0.13), $RuTFPPCl_8(CO)H_2O$ (0.20),[19] and $CuTFPPBr_8$ (0.16 Å).[23] Extended to the porphyrin periphery, this results in the second halogen atom of each pyrrole being significantly farther out of the plane than the first; in $ZnTFPPCl_8$ the displacements differ by 0.31 Å. Figure 4 shows the increase of both modes of distortion through the copper porphyrin series. The largest twist distortion is observed in the structure of $NiTFPPBr_8$,[23] likely due to the short nickel–nitrogen bond length (1.902 Å).[35,36]

A final measure of distortion is one based on the phenyl dihedral angles; to minimize steric contact with the β-substituents, the phenyl rings rotate toward the mean porphyrin plane (Figures 3 and 4). The dihedral angles decrease along the series H_2TFPP (79), $H_2TFPPCl_8$ (73), and $H_2TFPPBr_8$ (54°).

NMR Spectra. Fluorine-19 NMR has been extremely helpful in ascertaining both the identity and purity of halogenated compounds. The 100% natural abundance of spin $^1/_2$ ^{19}F and its high gyromagnetic ratio allow ^{19}F NMR spectra to be obtained readily.[37] As observed in ^1H NMR of tetraphenylporphyrins, the corresponding fluorine atoms from all four phenyl

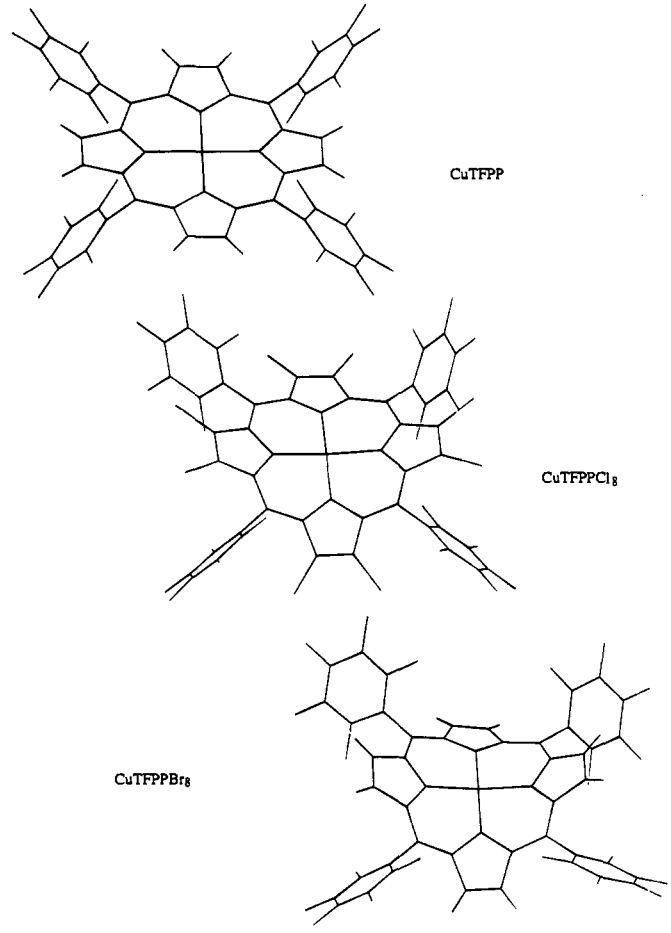

Figure 4. Molecular representations of the series CuTFPP, $CuTFPPCl_8$, and $CuTFPPBr_8$ using the crystal structure coordinates. Both saddle and twist distortions increase in the octachloro and octabromo derivatives.

Table 4. Average Deviation (Å) of Atoms from Least-Squares Plane

	$H_2TFPPCl_8$	$ZnTFPPCl_8$	$H_2TFPPBr_8$	H_2TFPP	ZnTFPP	CuTFPP
N	0.088	0.10	0.076	0.00	0.00	0.00
C_m	0.023	0.13	0.091	0.039	0.040	0.026
C_β	0.625	0.79, 0.68	0.903	0.071	0.074	0.051
Cl1 (Br1)	1.06	1.17	1.59			
Cl2 (Br2)	1.06	1.48	1.85			

rings appear equivalent in ^{19}F NMR. The four phenyl rings on the porphyrin are related in the high degree of symmetry of the approximate D_{4h} or D_{2d} point groups of these compounds. The chemical shifts of the fluorine atoms on the *meso*-phenyl rings are extremely sensitive to the metal center, its axial ligands, and the pyrrole carbon substituents however, such that each porphyrin will have a unique spectrum. Here we describe several correlations in ^{19}F shifts and splitting patterns as they relate to various TFPP structures.

The ^{19}F NMR spectra for the unmetalated and zinc TFPP and $TFPPX_8$ complexes (Figure 5; Table 5) display one set of signals each for the ortho, meta, and para fluorines. The para signal, identified by its intensity of $^1/_2$ relative to the ortho and meta signals, is most sensitive to metalation and shifts 1.7 ppm upfield from $H_2TFPPCl_8$ to $ZnTFPPCl_8$. The para resonance in the zinc and free-base octabromoporphyrins shows a similar shift in magnitude, with the largest shift upon metalation of H_2TFPP. The signal appears as a triplet due to coupling to the meta fluorines ($^3J_{F-F} = -21$ Hz). The ortho signal, farthest downfield, is split into a doublet of doublets, and the meta is a triplet of doublets. The additional splitting is attributed to coupling of fluorines positioned para to one another, as only

(35) Suh, M. P.; Swepston, P. N.; Ibers, J. A. *J. Am. Chem. Soc.* **1984**, *106*, 5164–5171.
(36) Hoard, J. L. In *Porphyrins and Metalloporphyrins*; Smith, K., Ed.; Elsevier: Amsterdam, 1975; pp 325.
(37) Harris, R. K. *Nuclear Magnetic Resonance Spectroscopy*; Pitman Publishing, Inc.: Marshfield, MA, 1983.

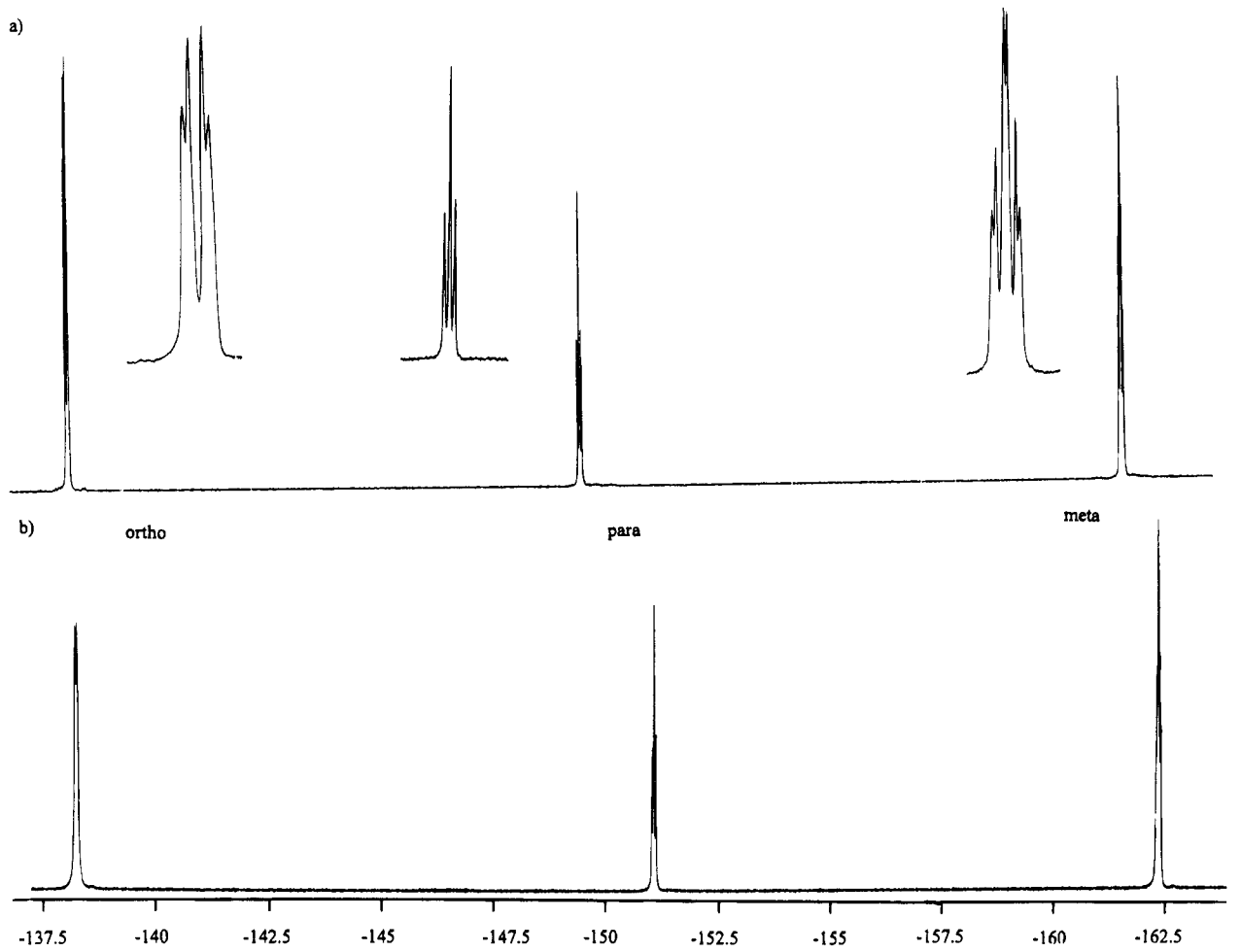

Figure 5. ^{19}F NMR spectra of (a) $H_2TFPPCl_8$ and (b) $ZnTFPPCl_8$ in $CDCl_3$. The signals are assigned ortho, para, meta, from left to right. The signals for the free ligand have been enlarged to show the fine structure observed in the spectra of free ligand, zinc, and other diamagnetic metal porphyrins.

Table 5. NMR Shifts for Halogenated Porphyrins

	NMR values in acetone-d_6[a]				
	^{19}F			^1H	
compd	ortho	para	meta	NH	β-H
ZnTFPP	−138.5 (d)	−154.8 (t)	−163.7 (m)		9.17
H_2TFPP	−136.9 (d)	−151.7 (t)	−161.8 (m)	−2.91	9.40
NiTFPP	−138.4 (d)	−153.7 (t)	−163.2 (m)		*b*
FeTFPP(Cl)	−105.8, −107.7	−150.2	−153.9, −156.0		83
FeTFPP(OH)	−108.0, −114.5	−152.0	−156.6, −158.0		83
$(FeTFPP)_2O$	−133.3, −137.1	−154.8	−163.1, −164.7		14.3
CuTFPP	not observable[d]				
$ZnTFPPCl_8$	−138.9 (d)	−151.5 (t)	−163.4 (m)		
$H_2TFPPCl_8$	−140.0 (d)	−149.8 (t)	−162.4 (m)	−1.0[c]	
$RuTFPPCl_8(CO)$[e]	−138.8, −139.3	−151.3 (t)	−163.2, −163.6		
$RuTFPPCl_8(py)_2$	−136.9 (d)	−149.7 (t)	−161.1 (m)		
$ZnTFPPBr_8$	−138.4 (d)	−151.7 (t)	−163.4 (m)		
$H_2TFPPBr_8$	−139.7 (d)	−150.1 (t)	−162.7 (m)	−0.5[c]	
$FeTFPPBr_8(Cl)$	−121.4, −122.3	−146.5	−158.1, −158.5		
$[FeTFPPBr_8(Cl)]^-$	−124, −133	−148	−158, −160		
$FeTFPPBr_8(py)_2$[f]	−138.6 (d)	−152.0 (t)	−163.1 (m)		

[a] ^{19}F NMR values are versus $CFCl_3$ at 0 ppm. ^1H NMR values are versus TMS at 0 ppm. Fine structure given as follows: (d) doublet of doublets, (t) triplet, (m) multiplet. [b] Not measured. [c] Very broad; the inner nitrogen protons are much more distinct in chlorocarbon solvents such as $CDCl_3$. [d] Cu(II) species are not generally observable due to their long relaxation time. [e] Major set of resonances, each with fine structure as observed in diamagnetic species; other resonances also observed, as discussed in text. [f] Values in $CDCl_3$.

the para signal does not show any additional structure, with $^5J_{F-F} = 6.7$ Hz. Computer simulation of the observed spectrum with only these parameters was not satisfactory. Additional coupling between meta fluorines of $^4J \approx -2$ Hz is needed to increase line width and generate the proper intensities in the model spectrum. The signs of the coupling constants are consistent with literature values, as are the magnitudes of the various J's (ortho > para > meta).[38]

Substitution with a paramagnetic or an axially unsymmetric metal center results in significantly different NMR spectra. High-spin, five-coordinate $Fe^{III}TFPP(Cl)$ (Figure 6) and FeTFPP(OH) samples, identified by their characteristic UV−vis and EPR spectra,[28] show *five* separate ^{19}F NMR signals that fall over a much larger window than those of the diamagnetic porphyrins. The ortho and ortho′ (and meta and meta′) fluorines, no longer related by an S_4 axis, now have chemical shifts separated by several ppm, and previously observed fine structure is lost due to paramagnetic line broadening. The resonances do not coalesce at temperatures up to 298 K, indicating that rotation of the phenyl rings is slow on the NMR time scale at room temperature.

The axial ligand is known to affect the ^1H NMR shifts of paramagnetic Fe^{III} porphyrins. In general terms, the porphyrin and the axial ligand compete for bonding interactions with the metal, and the strength of these interactions affects the ring current and π electron density on the protons and therefore their chemical shift.[39] A substantial downfield shift of all five resonances (Table 5) is observed upon substitution of an OH^-

(38) Bovey, F. A.; Jelinski, L. *Nuclear Magnetic Resonance Spectroscopy;* 2nd ed.; Academic Press, Inc: San Diego, CA, 1988; pp 437−488.
(39) Caughey, W. S.; Johnson, L. F. *J. Chem. Soc., Chem. Commun.* **1969**, 1362−1363.

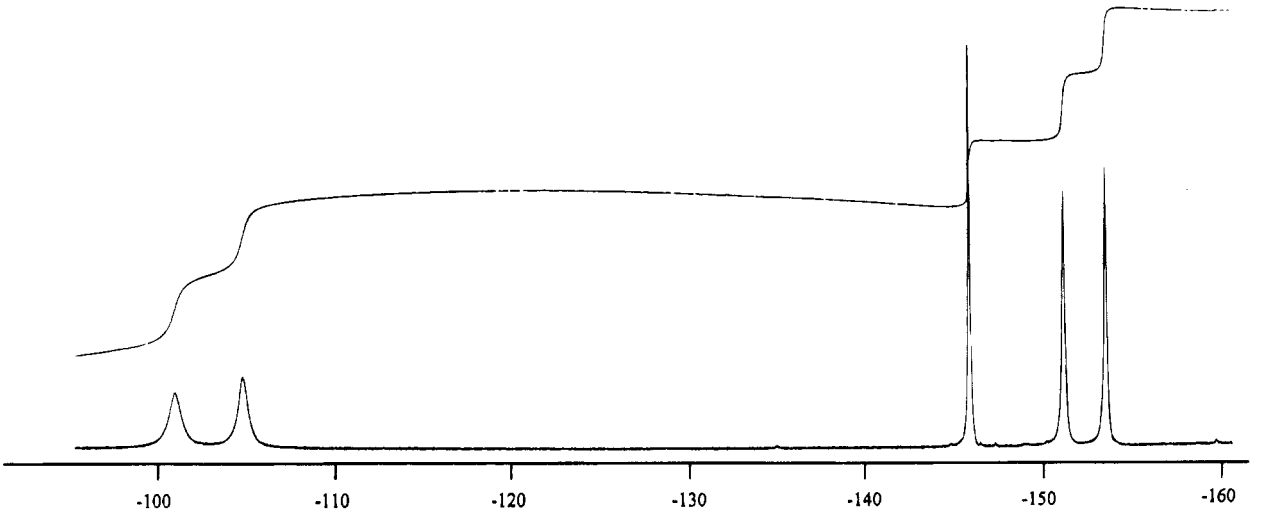

Figure 6. ^{19}F NMR spectrum of $Fe^{III}TFPP(Cl)$. The ortho resonances are shifted over 20 ppm downfield from those of H_2TFPP.

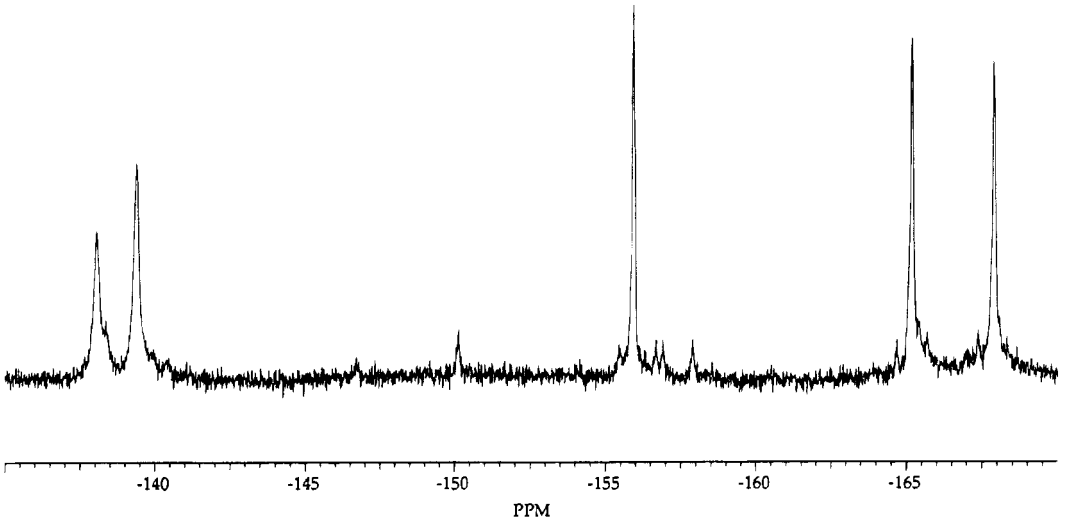

Figure 7. ^{19}F NMR spectrum of $(Fe^{III}TFPP)_2O$ in acetone-d_6. The window is much smaller than that for the paramagnetic FeTFPP(Cl) monomer due to antiferromagnetic coupling between the two iron atoms.

for a Cl^- ligand on $FeTFPP^+$, consistent with axial ligand effects observed with p-CH_3-TPPMn(X) complexes. Increased π bonding between the metal and the stronger field axial ligand reduces π electron density in the porphyrin, resulting in smaller contact shifts in the ^1H NMR spectrum.[40] Although the direction of the shift is similar in the fluorine spectrum, different magnitudes for the contact shift at the ortho and para positions relative to the meta are not observed. Therefore, contact shift alone is not sufficient to explain the ^{19}F NMR spectrum, which is consistent with the large temperature-independent paramagnetic term contributing to fluorine chemical shifts. Further study involving additional compounds would be needed to fully explore this effect.

The five-coordinate $(FeTFPP)_2O$ dimer also shows five peaks in its NMR spectrum (Figure 7); however, the signals show significantly less broadening and appear in a much narrower window than those of the other Fe^{III} porphyrins. Strong antiferromagnetic coupling between the two metal centers[28] reduces the paramagnetic shift in the ^{19}F NMR of the μ-oxo dimer.

The distinctive patterns observed in ^{19}F NMR play important roles in the structural assignment of other perhalogenated compounds. The ^{19}F NMR spectrum of $Fe^{III}TFPPBr_8(Cl)$ (Figure 8) shows a broadened five-signal pattern similar to that of FeTFPP(Cl). The ortho fluorine resonances exhibit a smaller paramagnetic shift in the perhalogenated compound. The addition of pyridine to $Fe^{III}TFPPBr_8(Cl)$ results in reduction of the iron and formation of the symmetric bis(pyridine) compound $Fe^{II}TFPPBr_8(py)_2$. The identification of this compound was confirmed as low-spin iron(II) due to the sharp signals and splitting pattern consistent with an axially symmetric, diamagnetic species. Most unusual is the NMR of $[Fe^{II}TFPPBr_8(Cl)]^-$, produced by electrochemical reduction of $Fe^{III}TFPPBr_8(Cl)$. The relatively sharp signals support the reduction of the metal center, but the splitting of the ortho and meta signals suggests an axially unsymmetric porphyrin; the Fe(II) porphyrin appears to retain an association with the chloride ligand even in the reduced state.[13]

NMR also revealed interesting properties of $RuTFPPCl_8(CO)$-H_2O.[19] Although an X-ray structure for this compound was obtained, ^{19}F NMR on dissolved crystalline material fails to yield a simple spectrum. Instead, several five-signal patterns are observed, suggesting that the strong trans effect of the carbonyl ligand results in lability of the sixth ligand. The unsymmetric trans coordination around the Ru again leads to dual ortho and meta signals (as in FeTFPP(Cl)), but with the diamagnetic metal center, the fine structure is retained. Upon photolysis in

(40) La Mar, G. N.; Walker, F. A. *J. Am. Chem. Soc.* **1975**, *97*, 5013–5106.

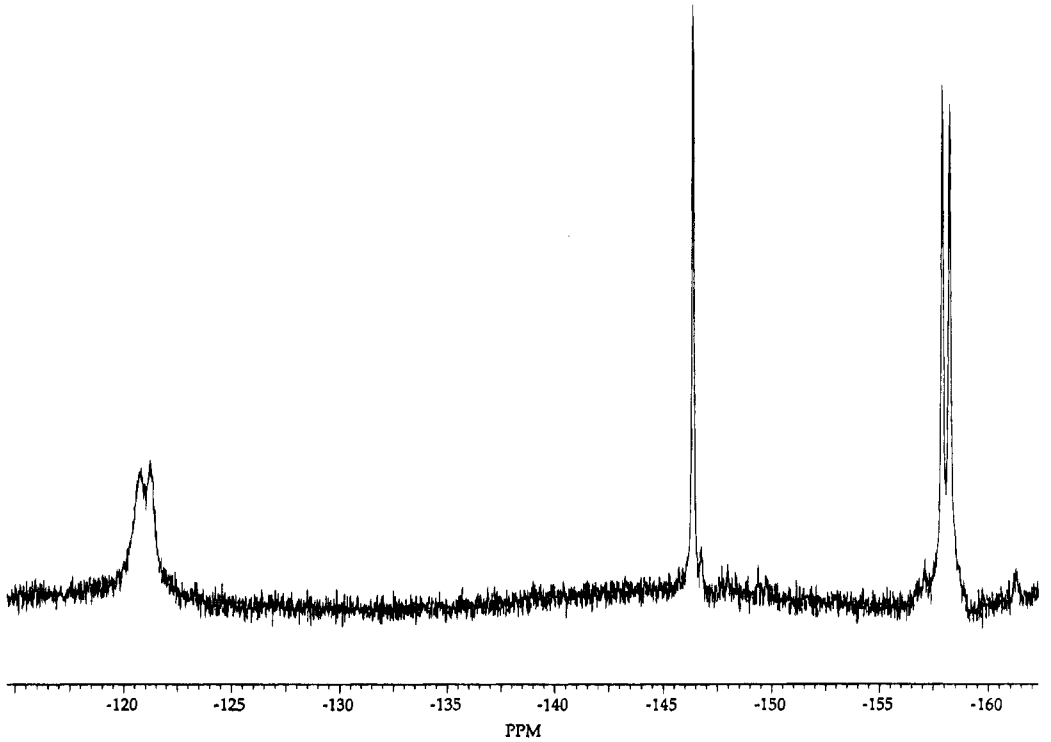

Figure 8. ^{19}F NMR spectrum of $Fe^{III}TFPPBr_8(Cl)$ in acetone-d_6. The paramagnetic shift is less than that for the partially halogenated FeTFPP(Cl).

pyridine, a single species, $RuTFPPCl_8(py)_2$, is obtained. The simple pattern now seen in the ^{19}F NMR shows that previous overlapping signals were due to multiple species with varying ligands trans to the CO rather than partial decomposition or dehalogenation of the porphyrin macrocycle.

Conclusions

Crystal structures of the planar tetrakis(pentafluorophenyl)-porphyrins H_2TFPP, ZnTFPP, and CuTFPP do not show significant perturbations relative to the corresponding TPP structures. The molecular structures of octabromo-tetrakis-(pentafluorophenyl)porphyrin and unmetalated and zinc octachloro-tetrakis(pentafluorophenyl) porphyrins are consistent with other structures that demonstrate that halogenation of the pyrrole β-carbons causes a severe saddling of the porphyrin macrocycle. The free base porphyrins, however, do not show the twisting distortion seen in the metalated octahalo derivatives, suggesting that the metal plays a significant role in determining the type and degree of distortion.

The distortions and metal effects observed in the structures of the halogenated metalloporphyrins are analogous to those reported for octamethyl and octaethyl derivatives of TPP: 2,3,7,8,12,13,17,18-octa-β-alkyl-5,10,15,20-tetraphenylporphyrin ($TPPX_8$, X = methyl, ethyl).[41,42] $ZnTPPMe_8$ and $ZnTPPEt_8$ are essentially the steric analogs of $ZnTFPPCl_8$ and $ZnTFPPBr_8$, respectively. The implication is that the observed distortion is a result of the steric interactions involving the β-halo substituents and is not electronic in origin.

Fluorine-19 NMR has been shown to be a useful tool for characterization of perhalogenated porphyrin compounds. The identification of various $FeTFPP(X)^+$ species will allow another mechanism to study catalysis reactions, for example, by monitoring deactivation of the catalyst via formation of a μ-oxo dimer. Trends in line widths, shift dispersions, and multiplicities all provide information on the oxidation state and coordination sphere of the metal center. As a supplement to crystallographic data, NMR allows a more direct examination of the behavior of these highly halogenated porphyrins in solution.

Experimental Section

Materials. Omnisol grade methanol, acetone, dichloromethane, benzene, dimethylformamide, and hexane were purchased from EM Science. *N*-Chloro- and *N*-bromosuccinimide, glacial acetic acid, iron(II) chloride, and triruthenium dodecacarbonyl were purchased from Aldrich and used as received. ZnTFPP and H_2TFPP were purchased from Porphyrin Products and used as received. UV−vis (CH_2Cl_2): ZnTFPP λ_{max} 414, 544 nm; H_2TFPP λ_{max} 412, 506, 584 nm. Fe^{III}-TFPP(Cl) was purchased from Aldrich and purified by chromatography on alumina before use. UV−vis (acetone): λ_{max} 350, 408, 500, 596 nm.

Methods. UV−vis spectra were recorded on an HP8452 diode array interfaced to an IBM or a Cary-14 spectrophotometer with an Olis 3820 conversion system. Porphyrin purification was accomplished with alumina (Fluka alumina eluting with $CHCl_3/CH_3OH$) or silica (Analtech 150 Å pore, 75−100 Å particle size silica eluting with CH_2Cl_2/hexane) column chromatography. Further purification of the zinc porphyrin was accomplished with a Beckman HPLC system (126 dual pump and 166 single channel detector) on a Vydac C-18 reverse phase column with isocratic acetone/water elution. ^1H and ^{19}F NMR spectra were recorded on a Bruker AM-500 (tuned to 470.56 MHz for fluorine detection) instrument in $CDCl_3$ or deuterated acetone and referenced internally to C_6H_5F at −113.6 ppm (vs $CFCl_3$ at 0 ppm). Elemental analyses of the perhalogenated compounds were obtained, and varied greatly by compound. Results were not satisfactory, even for crystalline samples that were pure by other criteria.

CuTFPP and NiTFPP. Copper and nickel were inserted into H_2-TFPP with metal(II) chloride salts by standard methods.[43] UV−vis (CH_2Cl_2): CuTFPP λ_{max} 408, 534, 576 nm; NiTFPP λ_{max} 406, 526, 560 nm.

$Fe^{III}TFPP(OH)$ and $(Fe^{III}TFPP)_2O$. $Fe^{III}TFPP(OH)$ and $(Fe^{III}$-$TFPP)_2O$ were synthesized from the chloride by published methods:[28]

(41) Sparks, L. D.; Medforth, C. J.; Park, M.-S.; Chamberlain, J. R.; Ondrias, M. R.; Senge, M. O.; Smith, K. M.; Shelnutt, J. A. *J. Am. Chem. Soc.* **1993**, *115*, 581−592.

(42) Barkigia, K. M.; Berber, M. D.; Fajer, J.; Medforth, C. J.; Renner, M. W.; Smith, K. M. *J. Am. Chem. Soc.* **1990**, *112*, 8851−8857.

(43) Adler, A. D.; Longo, F. R.; Kampas, F.; Kim, J. *J. Inorg. Nucl. Chem.* **1970**, *32*, 2443−2445.

$Fe^{III}TFPP(Cl)$ was dissolved in benzene, and a small amount of NaOH solution was added. After several hours of stirring, the water was removed with a separatory funnel, and the benzene solution was chromatographed on neutral alumina with a benzene/acetone solution. The μ-oxo elutes first, and the hydroxide elutes with a higher percent acetone. $Fe^{III}TFPP(OH)$: UV−vis (acetone) λ_{max} 406, 563 nm. $(Fe^{III}TFPP)_2O$: UV−vis (CH_2Cl_2) λ_{max} 398, 415 (shoulder), 560 nm.

$H_2TFPPCl_8$. Chlorination of ZnTFPP was accomplished by a modification of earlier methods.[2,4,44] Approximately 500 mg of ZnTFPP was dissolved in 50 mL of dry methanol with 40 equiv of *N*-chlorosuccinimide, and the mixture was refluxed for 1 h. When chlorination of the pyrrole positions was complete, as determined by the red shift of the Soret band in the UV−vis and thin-layer chromatography on silica plates (1:1 hexane/dichloromethane), the solution was allowed to cool. The product was precipitated with water, filtered, and washed with cold hexane to remove decomposed porphyrin byproducts. Further purification by HPLC was necessary to separate partially chlorinated species. Yield of $ZnTFPPCl_8$: 60−80%. UV−vis (CH_2Cl_2): λ_{max} 364, 442 (Soret), 576 nm. Mass spectrum: m/z = 1314 (calcd 1313). The chlorinated zinc porphyrin was demetalated as previously done by Lyons et al.:[4] $ZnTFPPCl_8$ was redissolved in approximately 50 mL of chloroform, and HCl gas was passed through a gas dispersion tube into the solution for 1−2 min. The volume of the reaction mixture was reduced, and the solution was chromatographed on alumina, eluting with 95% chloroform−5% methanol. The product, $H_2TFPPCl_8$, was collected and rotary-evaporated to dryness, with a yield of approximately 95%. UV−vis (CH_2Cl_2): λ_{max} ($\epsilon/10^4$); 436 (16), 536 (1.3), 622 nm (0.46).

$H_2TFPPBr_8$. The bromo analog was similarly synthesized via bromination of ZnTFPP with *N*-bromosuccinimide. $ZnTFPPBr_8$: UV−vis (CH_2Cl_2) λ_{max} ($\epsilon/10^4$) 455 (18), 585 (2.7) nm. The free ligand was obtained by demetalation with HCl gas, and the product was chromatographed on alumina. UV¬vis (CH_2Cl_2): λ_{max} 454, 552, 636 nm.

$FeTFPPBr_8(Cl)$. Iron was inserted into $H_2TFPPBr_8$ with freshly prepared iron(II) acetate in glacial acetic acid[45] or with $Fe^{II}Cl_2$ in DMF.[43] Insertion was evident by the red color of the solution. The iron porphyrin was precipitated with brine, dried, and washed with hexane to remove impurities. UV−vis (CH_2Cl_2): λ_{max} ($\epsilon/10^4$) 402 (8.1), 442 (8.5), 560 nm (1.4). Addition of pyridine to a solution of $FeTFPPBr_8(Cl)$ led to formation of $Fe^{II}TFPPBr_8(py)_2$. UV−vis (CH_2Cl_2): λ_{max} 450, 556, 588 nm.

$RuTFPPCl_8(CO)H_2O$. Ruthenium was inserted into $H_2TFPPCl_8$ with $Ru_3(CO)_{12}$ in refluxing hexafluorobenzene as previously described[19] and purified by silica gel column chromatography. UV−vis (CH_2Cl_2): λ_{max} ($\epsilon/10^4$) 416 (17), 542 (1.5).

Crystal Structure Analysis. A suitable single crystal was mounted in a capillary with silicone grease and centered on an Enraf-Nonius CAD-4 diffractometer using Mo Kα radiation. Atomic scattering factors and values for f' were taken from Cromer and Waber[46] and Cromer,[47] and CRYM,[48] MULTAN[49] ($ZnTFPPCl_8$ only), and ORTEP[50] computer programs were used for calculations. The weights were taken as $1/\sigma^2(F_o^2)$; variances ($\sigma^2(F_o^2)$) were derived from counting statistics plus an additional term, $(0.014I)^2$; variances of the merged data were obtained by propagation of error plus another additional term, $(0.014\bar{I})^2$.

Crystals of H_2TFPP (red-brown) and CuTFPP (red) were grown via the slow evaporation of a methylene chloride solution over a period of several days. CuTFPP crystallized in space group $R\bar{3}$, the copper coordinates were obtained from a Patterson map, and the remaining non-hydrogen positions were determined from structure factor and Fourier calculations. H_2TFPP was found to be isostructural; hydrogen atom coordinates were found in difference maps. X-ray-quality crystals of ZnTFPP (pink) were grown by diffusion of hexane in chloroform. The zinc crystal was found to belong to the monoclinic space group $P2_1/c$. The zinc atom, located from a Patterson map, was placed at $^1/_2$, $^1/_2$, $^1/_2$; one structure factor Fourier cycle showed the remaining carbon and nitrogen atoms of the porphyrin. The hexane molecule appeared in the subsequent cycle. The hydrogen atoms were positioned by calculation (staggered geometry, C−H = 0.95 Å) and kept fixed but were adjusted prior to the final least-squares cycle.

Brown crystals of $H_2TFPPCl_8$ were grown by slow evaporation from an acetone/water solution. The crystals were found to be triclinic, belonging to space group $P\bar{1}$. The structures were solved with MULTAN, and the two inner hydrogen atoms were located in a difference map as disordered among the four nitrogen atoms. Their positional parameters were refined, with B values fixed at 1.2 times the isotropic equivalent U_{ij} value of the bonded nitrogen atoms and the population factors assigned at one-half. Purple crystals of $ZnTFPPCl_8$ were grown from a saturated solution of *o*-dichlorobenzene at 0 °C. Crystals of this compound lost solvent quickly, so one was covered with epoxy glue before being cooled to −44 °C on the diffractometer. The zinc crystal was found to be tetragonal, belonging to space group $P\bar{4}2_1c$. The structure was solved by location of the zinc atom from a Patterson map. Structure factors and Fourier calculations showed Cl1 and Cl2, and subsequent structure factor Fourier calculations gave the rest of the porphyrin. Solvent molecules were found in difference Fourier maps calculated in their planes. The solvent molecules occupy two separate regions in the cell, each region holding one dichlorobenzene molecule. The molecules are disordered in these regions, and were initially modeled with idealized $C_6H_4Cl_2$ groups. Eventually, some of the chlorine atoms of the solvent were refined, as well as the population parameters for alternate orientations, but the carbon atoms were always positioned on the basis of Fourier maps. For one region (C31−36 and C41−46) anisotropic displacement parameters were assigned by hand based on the maps and the refined parameters of the Cl atoms of the solvent; the other carbon atoms of the solvent were left isotropic. The disordered solvent regions are the cause, in all probability, of the somewhat larger than usual values for R and goodness of fit.

Brown crystals of $H_2TFPPBr_8$ were grown via the slow evaporation of a 9:1 solution of methylene chloride/*o*-dichlorobenzene. The structure (space group $C2$) was solved from the Patterson map with subsequent structure factor−Fourier cycles. The carbon atoms of the solvent were not refined but were repositioned once near the end of refinement based on a Fourier map calculated in their plane. The two hydrogen atoms presumed to be on the nitrogen atoms were not located.

Acknowledgment. We thank Mike Hill for helpful discussions and assistance with certain experiments. This work was supported by the National Science Foundation, the U.S. Department of Energy, Morgantown Energy Technology Center, the Gas Research Institute, and Sun Co., Inc. E.R.B. acknowledges the NDSEF for a graduate fellowship, and M.W.G. acknowledges the NIH for a postdoctoral fellowship.

Supporting Information Available: ORTEPs and tables of final heavy atom parameters, anisotropic displacement parameters, and complete distances and angles for H_2TFPP, ZnTFPP, CuTFPP, $H_2TFPPCl_8$, $ZnTFPPCl_8$, and $H_2TFPPBr_8$, tables of H atom parameters for H_2TFPP, ZnTFPP, CuTFPP, and $H_2TFPPCl_8$, tables of intermolecular distances less than 3.5 Å for ZnTFPP, $ZnTFPPCl_8$, and $H_2TFPPBr_8$, and tables of nonrefined parameters for $H_2TFPPBr_8$ (63 pages). Ordering information is given on any current masthead page.

IC9412825

(44) Hoffmann, P.; Robert, A.; Meunier, B. *Bull. Chem. Soc. Fr.* **1992**, *129*, 85−97.
(45) Warburg, O.; Negelein, E. *Z. Biochem.* **1932**, 14−32.
(46) Cromer, D. T.; Waber, J. T. *International Tables for X-ray Crystallography*; Kynoch Press: Birmingham, U.K., 1974; Vol. IV, pp 99−101.
(47) Cromer, D. T. *International Tables for X-ray Crystallography*; Kluwer Academic Publishers: Dordrecht, The Netherlands, 1974; Vol. IV, pp 149−151.
(48) Duchamp, D. J. Abstracts of Papers, American Crystallographic Association Meeting, Bozeman, MT, 1964; No. B14, pp 29−30.
(49) Debaerdemaeker, T.; Germain, G.; Main, P.; Refaat, L. S.; Tate, C.; Woolfson, M. M. *MULTAN 88. Computer Programs for the Automatic Solution of Crystal Structures from X-ray Diffraction Data*, Universities of York and Louvain: York, England, and Louvain, Belgium, 1988.
(50) Johnson, C. K. *ORTEPII*. Report ORNL-3794; Oak Ridge National Laboratory, Oak Ridge, TN, 1976.